Carbon Trends 7 (2022) 100157

Contents lists available at ScienceDirect

Carbon Trends

journal homepage: www.elsevier.com/locate/cartre

Bactericidal vertically aligned graphene networks derived from renewable precursor

Ahmed Al-Jumaili[a,b], Muhammad Adeel Zafar[a], Kateryna Bazaka[a,c], Janith Weerasinghe[d,e], Mohan V. Jacob[a,*]

[a] Electronics Materials Lab, College of Science and Engineering, James Cook University, Townsville, QLD 4811, Australia
[b] Medical Physics Department, College of Medical Sciences Techniques, University of Mashreq in Baghdad, Iraq
[c] Research School of Electrical, Energy and Materials Engineering, The Australian National University, Canberra, ACT 2601, Australia
[d] School of Chemistry and Physics, Queensland University of Technology (QUT), Brisbane, QLD 4000, Australia
[e] Centre for Materials Science, Queensland University of Technology (QUT), Brisbane, QLD 4000, Australia

ARTICLE INFO

Article history:
Received 16 September 2021
Revised 23 December 2021
Accepted 24 January 2022

Keywords:
Graphene
PECVD
Antibacterial
Vertical graphene

ABSTRACT

Graphene nanostructures exhibit a wide range of remarkable properties suitable for many applications, including those in the field of biomedical engineering. In this work, plasma-enhanced chemical vapor deposition was utilized at different applied RF power for the fabrication of vertical graphene nanowalls on silicon and quartz substrates from an inherently volatile carbon precursor without the use of any catalyst. AFM confirmed the presence of very sharp exposed graphene edges, with associated high surface roughness. The hydrophobicity of the material increased with the power of deposition, reaching the water contact angle of 123 ° for 500 W. Confocal scanning laser microscopy demonstrated that the viability of gram-negative *Escherichia coli* and gram-positive *Staphylococcus aureus* cells were 33% and 37% when incubated on graphene samples, respectively, compared to controls (quartz) that showed the viability of 82% and 84%, respectively. SEM verified significant morphological damage to bacterial cell walls by the sharp edges of graphene walls, with cells appearing abnormal and deformed. The presented data clearly contributed to the current understanding of the mechanical-bactericidal mechanism of vertically oriented graphene nanowalls upon direct contact with microorganisms.

1. Introduction

Graphene-based structures continue to be broadly studied across multiple areas of research due to their exceptional characteristics, which are derived from the single-atom-thick sp^2-bonded carbon atoms densely assembled in a honeycomb crystal lattice [1]. Graphene is considered to be the world's thinnest, strongest and most conductive 2D structure with high surface area (2630 m^2/g), super hydrophobicity (~150°) and high optical transmittance of around 97% over the entire wavelength region [2,3]. These extraordinary features have promoted the integration of graphene into various fields ranging from advanced electronic, energy generation and storage, sensors, flexible displays, efficient solar panels, to drug delivery and biomedical applications. The surface ordering of graphene sheets is of utmost importance for successful usage [4,5]. Yet, some issues may arise when graphene sheets are randomly assembled on a substrate, promoted by the high tendency of graphene sheets to permanently agglomerate, or restack owing to the powerful $\pi-\pi$ stacking and van der Waals forces [6]. Such issues could prevent graphene sheets from fully interacting with their environment, directly affecting their performance in such applications as sensing, supercapacitors and biomaterials [7,8].

Vertically oriented graphene nanowalls (VOGNs) control the manner in which graphene interact with their environment and maximize the exposure of the reactive edge and defects distributed across the sheet surface to the environment. VOGNs are a non-stacking 3D structure with lateral and vertical dimensions ranging from 0.1 nm to tens of micrometers, where each individual nanowall comprises few-layer graphene (1–10 layers) with an interlayer spacing around 0.3 nm [8,9]. Compared to horizontal graphene, VOGNs have a higher density of reactive open edges, great surface-to-volume ratio, specific orientation with respect to the substrate surface, and non-stacking property. Importantly, VOGNs can be directly grown on the substrate. The definite

* Corresponding author.
E-mail addresses: ahmed.al-jumaili@uom.edu.iq (A. Al-Jumaili), Mohan.Jacob@jcu.edu.au (M.V. Jacob).

https://doi.org/10.1016/j.cartre.2022.100157

performance of VOGN structures is mainly reliant on its fundamental and morphological features including sharpness and length of the active edges, degree of interconnectivity between individual walls, dimensions, spacing between layers, existence of defects and/or dopants, etc.

From biological perspective, characteristics of VOGNs offer a promising potential to deactivate microorganisms. Indeed, several vertical graphene architectures have revealed wide-spectrum antimicrobial activities toward common human pathogens [10–13]. The antimicrobial performance of these structures is believed to be instigated by physical and/or chemical interactions upon direct contact with microbial cells [14]. Although bactericidal properties of VOGNs have been theoretically and experimentally investigated, their antibacterial mechanisms are still controversial. In a very recent study, Wei et al. examined the biocidal activities of vertically and horizontally oriented graphene developed on semiconductor and insulator substrates [15]. The outcomes revealed that a significant antibacterial activity was only achieved for vertical graphene grown on semiconductor substrates, indicating both the orientation of graphene and conductivity of underlying substrates highly influence the microbial inactivation [15]. Similarly, in another report that showed vertically grown graphene to have a powerful bactericidal performance, the penetration of graphene flasks into the affected microorganism was found to be highly depended on the angle between the graphene and the cell membrane [16]. Furthermore, vertically-oriented graphene nanosheets produced from different precursors also revealed effective antifouling activities toward pathogens (e.g., *E. coli* and *S. aureus*) [17].

The advantages of using vertically oriented graphene in mitigating microbial attachment on surfaces has been proven through experimental, theoretical and simulation studies [18,19]. Pandit et al. [16] demonstrated that monolayer horizontal graphene on surfaces did not affect bacterial cells, whereas, vertical graphene led to an extensive mechanical rupturing of bacterial cells. The nanosheets of vertical graphene act as “nano-knives”, which cause localized piercing of the cell membrane, leading to the leakage of cellular contents and ultimately killing the bacteria [20]. Another work explained bacterial lysis by means of local disruption of a bacterial lipid bilayer which obstructs cellular metabolism and causes cell death [21]. Furthermore, it has been found that vertical graphene is equally effective against both Gram-negative and Gram-positive bacteria [22].

Plasma-assisted technology can be utilized to produced graphene walls that do not collapse or agglomerate, where their properties (e.g., orientation, density of networks, thickness of walls) are controlled via growth parameters. Among fabrication methods, plasma enhanced chemical vapor deposition (PECVD) is a bottom-up technique that is highly versatile and feasible for large-area production of vertical graphene structures at reasonable growth rates [23,24]. PECVD can yield dense carbon nanoflakes/nanowalls without using any catalyst, which ensures higher purity compared to other production techniques [25]. It also allows for the preservation of original minerals existing in the precursor, resulting in varying morphologies and chemistries of the resultant graphene [26]. The properties of graphene produced by PECVD highly depends on the processing parameters, (e.g., catalyst, applied power, temperature, reactive gas, pressure, precursor, growth time and substrate coating), which should be carefully optimized. In catalyst-free PECVD system, the plasma power is a key parameter determining the dissociation of reactant molecules and regulates the density, momentum and energy of the plasma species (ions, electrons and neutral species) inside the bulk plasma. Indeed, the plasma field are effective in breaking the bonds of carbon-based precursors decreasing the required temperature for graphene fabrication.

This study investigates the physical bactericidal mechanism of VOGNs toward pathogenic bacteria by fabricating graphene with dissimilar edge densities. The VOGNs were produced at different radio frequency (RF) powers using a single-step catalyst-free PECVD system. The RF powers applied for the syntheses of vertically aligned graphene were 300, 400 and 500 W, where the resulting samples abbreviated as VG 300, VG 400, and VG 500, respectively. To the best of our knowledge, this is first work systematically investigates the antimicrobial activities of VOGNs films derived from the essential oil family of precursors, namely the essential oil *P. graveolens*.

2. Experimental

2.1. Graphene synthesis

The graphene was fabricated using a single step RF-PECVD technique. The plasma reactor used in this study has been described elsewhere [27,28]. Briefly, the PECVD system, shown in Fig. 1, consists of a quartz tube reactor with an external heater. An adjustable voltage regulator was utilized to obtain the required temperature of 700 °C. The starting pressure was kept around 0.05 mbar. Then, the pressure of the reactor was kept at 0.20 mbar when H_2 gas was flown at the rate of 10 sccm. Three input powers were used 300, 400, and 500 W, supplied using the Navio RF Generator operating at 13.56 MHz frequency through the Navio Matching Network. Prior to the deposition stage of the process, substrates were pretreated with hydrogen plasma for 1 min for surface preparation. The vaporized precursor was then introduced into the reactor using a manual flow controller. In all experiments, silicon (with 100 nm oxide layer) and quartz substrates (1×1 cm^2) were washed with acetone and propanol, and dried by air gun prior to the deposition. It is well known that the growth of vertical graphene by PECVD is a complex process, where the morphology, dimensions, phase, adhesion to substrate, degree of crystallinity, and density of graphene are highly influenced by the interrelated growth parameters [6,29]. Thus, we kept all processing parameters identical during all experiments, and only changed the power of deposition. The initial optimization of the home-made PECVD system suggested a hydrogen flow rate is 10 sccm, temperature is 700 °C, pressure is 0.2 mbar, and deposition duration is 4 min. Detailed information about the optimization procedure can be found in ref. [30].

It is worth mentioning that the synthesis of graphene from inexpensive natural precursors is of great interest from both an ecological and industrial point of view [31]. In the literature, VOGNs have successfully been derived from environmentally friendly low-cost precursors such as honey [32], butter [33], coconut oil [34], orange fruit, [35], biomass waste [36], milk and sugar [29]. The use of other precursors such as volatile plant extracts has received less attention. Secondary metabolites harvested from plants are renewable substances suitable for producing graphene through PECVD, since they are carbon-rich volatile oily liquids that evaporate at room temperature without any carrier gas [5,37]. A previous study reported successful synthesis of VOGNs from *Melaleuca alternifolia* utilizing green catalyst-free low temperature PECVD. The resultant graphene material demonstrated high quality, enhanced surface area with ultra-long edges, great surface roughness, and a low level of defects [38]. In this study, the precursor (*Pelargonium graveolens*) was obtained from Australian Botanical Products (ABP, Victoria, Australia), and its vapors were introduced into the PECVD system without further modification. The selected precursor is a hydrocarbon-rich mixture containing more than 80 components; mainly citronellol ($C_{10}H_{20}O$) and geraniol ($C_{10}H_{18}O$) [39,40].

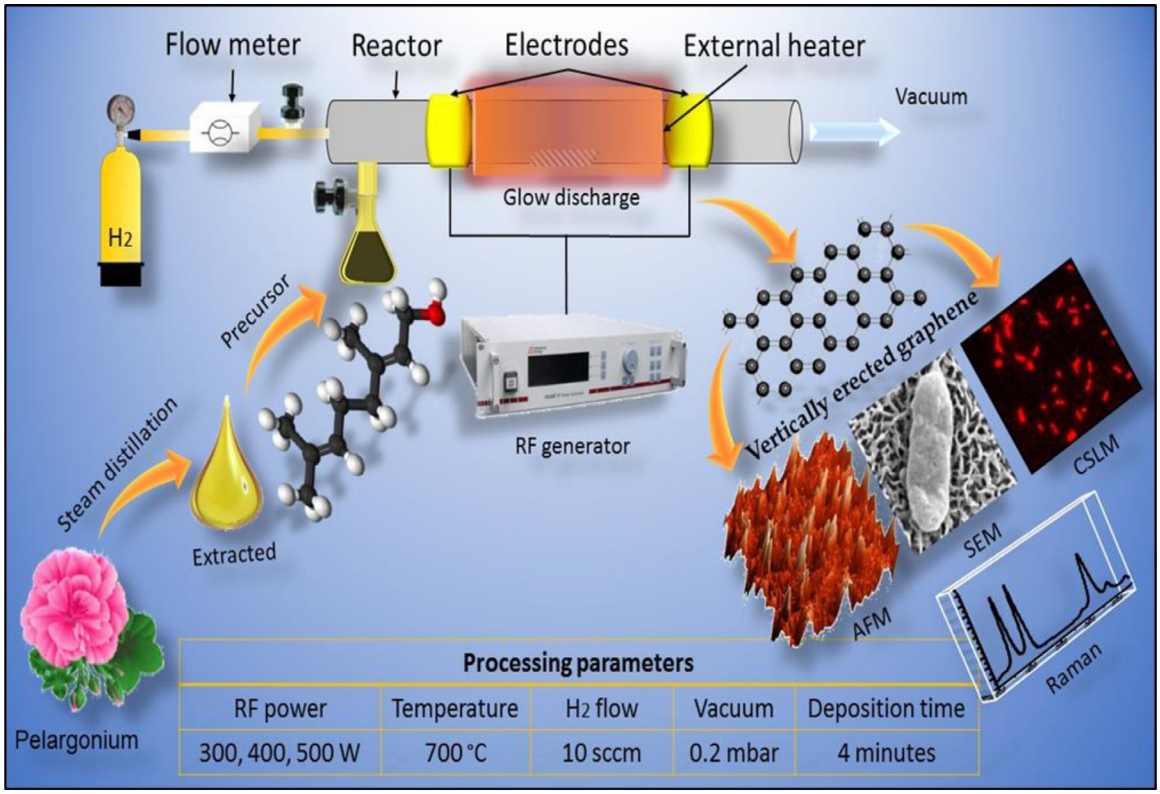

Fig. 1. Overview of the fabrication process and the representative features of vertically oriented graphene nanowalls produced by plasma enhanced chemical vapor deposition.

2.2. Graphene characterization

Raman measurements were performed in an ambient environment at room temperature using a WITec's Raman spectrometer (WITec, Ulm, Germany) with the laser excitation wavelength of 532 nm. X-ray photoelectron spectroscopic studies (XPS) were carried out using a Specs SAGE 150 spectroscope enhanced with an Al Kα X-ray (E = 1486.6 eV) monochromatic source. XPS spectra were acquired at 90°angle from a circular spot (diameter = 5 mm). In order to decrease any potential damage to the investigated samples, the exposure period was kept as minimal as possible to obtain sufficient signal-to-noise ratio. Static water contact angle measurements were recorded using a goniometer (KSV CAM 101, Helsinki, Finland). Young–Laplace fitting was used to estimate the contact angle and a minimum of three measurements per sample were obtained. Surface morphology was inspected using a high-resolution and low-noise scanning atomic force microscope (AFM) (NT-MDT NTEGRA, Moscow, Russian Federation) with a scanning area of 5 µm × 5 µm. AFM was used in the tapping mode. The data then analyzed using Nova Software (Version 1.0.26, Moscow, Russian) with the fitting adjustment value (polynomial order of 4). Scanning Electron Microscopy (SEM) (SU5000, Hitachi, Canada) was also employed to image VG samples fabricated on silicon substrates at V_{acc} = 3.0 kV, EC = 124 K nA and WD = 9.0 mm. Transmission electron microscopy (TEM, JEOL 2100, JEOL Ltd., Tokyo, Japan) was used to analyze the morphology of the graphene.

The antibacterial effectiveness of VG toward gram-negative *Escherichia coli* and gram-positive *Staphylococcus aureus* cells was evaluated by Live/Dead staining and visualization. The experiment was run in triplicate. For each test, a fresh bacterial suspension was prepared by first refreshing the frozen stock culture (1 mL) in Oxoid nutrient broth (10 mL) at 37 °C in shaking mode at 120 rpm. A spectrometer instrument (The SPECTROstar Nano, BMG labtech, Germany) was used to estimate bacterial concentration prior to placing them onto graphene surfaces. The cell mass was kept at 0.1 at optical density of 600 nm to produce a uniform starting culture of 2 × 10^5 cell/ CFU. Controls (quartz substrates) and VG samples were placed into 12-well plates, then treated by UV light for 20 min on each side to sterilize the samples. An aliquot of 2 ml of bacterial suspension was placed onto the sample surface. All tested samples were incubated at 37 °C and 5% CO_2 for 24 h. After the incubation period, a staining kit (SYTO^{TM} Invitrogen, Thermo Fisher, USA) was applied to study live/dead microbial cells. The dyes were used following the protocol defined in [41]. Prior to imaging of the cells retained on sample surfaces, bacterial suspensions were gently removed from the samples. Then, 90 μl of the stain was gently placed on top of each sample and the samples were covered with metal foil. After 20 min, samples were lightly washed with 0.5 ml of distilled water to remove unattached bacteria. Fluorescent images were acquired with a confocal laser scanning microscope (LSM 800, ZEISS, Germany), with green and red signals corresponding to live and non-viable cells, respectively. Viability was assessed as the percentage of viable, adhering bacteria relative to the total number of bacteria attached to the surface.

To obtain SEM images, *E. coli* and *S. aureus* cells were cultured on surfaces of control, VG 300, VG 400, and VG 500 for 24 h at 37 °C at the densities described above. After the growth, the bacterial culture medium was gradually removed from wells and phosphate buffered saline (quantity of 2 ml) was used to wash each specimen. In order to dehydrate cells, each sample was subjected to a series of different ethanol concentrations applied in ascending order (30%, 50%, 70%, 80% and 100%), at 10 min per each concentration. Then, the dehydrated specimens were coated with a few nanometer-thick film of palladium metal using an ion sputter (deposition time of 60 s). This supplementary coating step is typically used to increase the bulk conductivity of samples and reduce

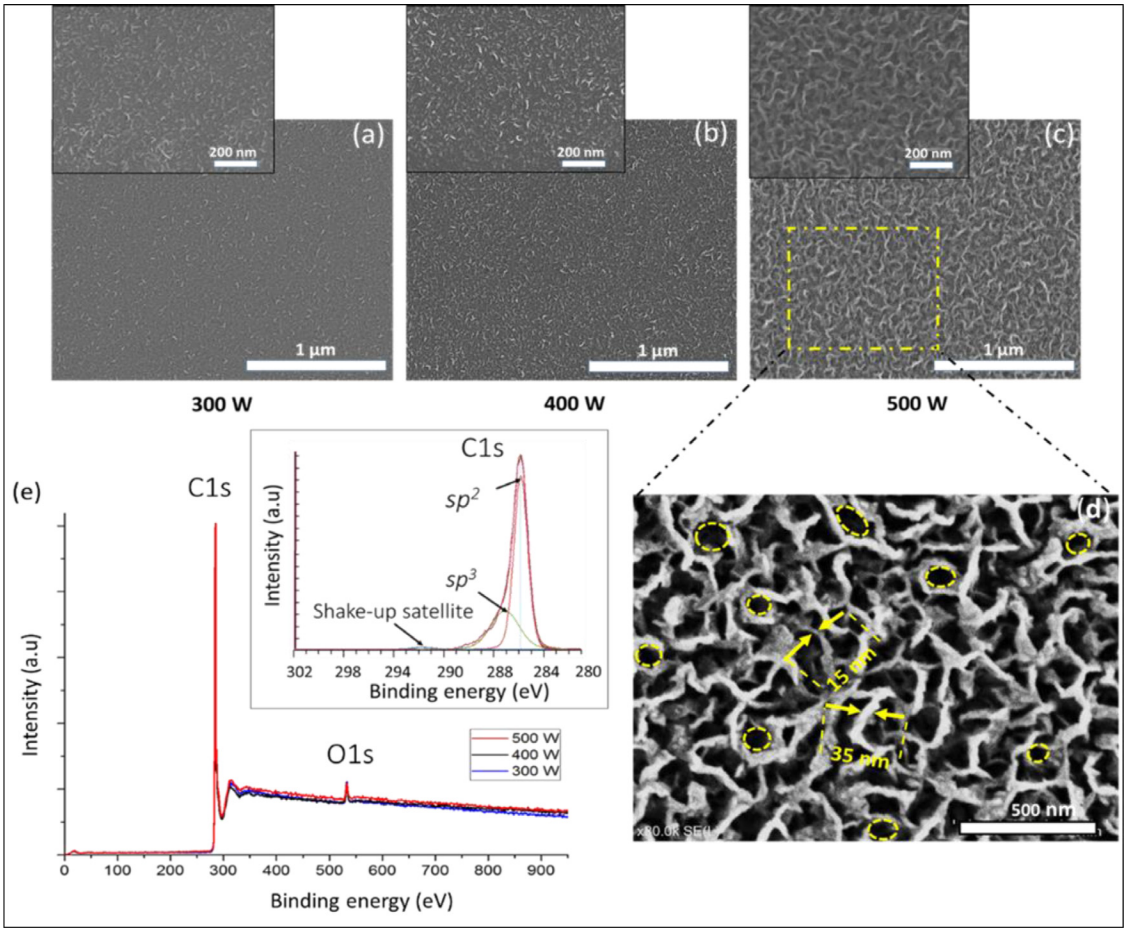

Fig. 2. (a), (b) and (c) SEM images acquired for VG samples produced at different RF processing powers. (d) High magnification SEM images of VG 500 sample. (e) Full XPS spectra of VG samples and associated deconvolution of C1s fitted with three sub-peaks (For interpretation of the references to color in this figure, the reader is referred to the web version of this article.).

charging on insulating surfaces (e.g., those of cells), which greatly enhances the ability to visualize bacterial cells at high magnifications.

3. Results and discussion

3.1. SEM and XPS

Microscopic observations of graphene synthesized at different power of deposition are shown in Fig. 2.a–d. At RF power of 300 W, the early growth phase of separated graphene nano-islands (Fig. 2.a) can be observed on the substrate initiating C sp^3-hybridized nucleation centers. The average size of each nano-island structure was ranging between 10 and 20 nm. When the power of deposition was increased to 400 W, a slight increase in the size of graphene islands was achieved, around 15 to 40 nm. The increase in the size of graphene islands at the higher applied power can be attributed to the greater dissociation rate of precursor molecules; in addition to an increase in the generated electrical field with successive carbon diffusion on the edges (due to strong in-plane C–C covalent bond). Although graphene structures formed at 400 W were greater in number, and larger in size with less interspacing area, they again did not fully cover the substrate (Fig. 2b). Nevertheless, with an increase in RF power to 500 W, significantly larger nanowalls were formed with an interconnected network configuration of graphene completely covered the substrate, as represented in Fig. 2c & d. The length of formed graphene walls was between 150 and 300 nm, with widths varied between 10 and 40 nm.

Upon increasing the applied RF power to 500 W, the density of formed graphene nano islands increased and those standing vertically on the substrate continued to grow faster. As active plasma continually generates carbon atoms, those nano islands coalesce, resulting in the creation of densely connected vertically standing maze-like architecture with sharp top boundaries [30,42]. We estimated the total length of the top edges in 1 cm^2 area of VG 500 sample as 2.4 ± 0.06 km using ImageJ software. In addition, several nano-cavities (circular shape) with an average radius 15 nm appeared among the graphene nanowalls (highlighted in yellow in Fig. 2.d).

SEM data emphasized the significant influence of RF power on the resultant graphene growth. When the RF is applied, the precursor molecules become subject to inelastic collisions with energetic plasma electrons, generating free radicals, ions, and other active species. Indeed, higher RF power yields a comparatively greater chemical potential gradient at the substrate surface by ion focusing effects; and hence fast supply of precursor fragments. At the same time, plasma field increases the temperature of the top surface of the substrate, which further enhances the subsequent precursor dissociation. Effects of substrate heating on the dynamics of VG growth in PECVD has been discussed here [42].

The surface growth of graphene in a catalyst-free bottom-up scheme occurs by adsorption of C–H radicals onto the surface and creation of an amorphous carbon layer (with some graphitic struc-

tures) on the substrate. Due to ion bombardment, defects and immobilized free radical (dangling bonds) are formed leading to the creation of active nucleation sites. Those active sites develop by migration of carbon species and development of nano-islands possessing large quantities of dangling bonds. The nucleation of graphene nano-sheets on dangling bonds initiates 2D structures with random orientations, which then act as a subsequent growth template. The available carbon atoms in the plasma continuously bond to the active edge of freshly formed graphene sheets. In particular, vertical structures that are perpendicular to the substrate surface develop faster (due to electric field effect) and shadow lower counterpart sheets, as a result the former sheets grow much faster, forming vertical graphene nanowalls.

Fig. 1.e presents full XPS spectra for graphene samples fabricated at several RF powers on SiO_2 substrates. The survey scan displayed a single shape peak at a binding energy of ~284 eV, which corresponds to C1s band demonstrating that the formed material is predominated by carbon atoms. Besides, a relatively lower intensity peak identified at ~531 eV corresponds to O1s band. The O1s probably arises owing to the exposure of graphene to the ambient air. Also, oxygen groups existing in the monomer components could be responsible for the detected oxygen bond [5]. Apart from oxygen, there were no signal of any impurities nor metal ions, signifying the absence of any catalyst in VOGNs formation.

The high resolution of XPS scan for C1s bond, presented in Fig. 2e, was analytically fitted with three sub-peaks. The deconvolution showed that the main peak at ~284.8 eV associates with sp^2 hybridized carbon (C=C) of graphitic crystal. Besides, a minor peak at 285.3 eV relates to sp^3 hybridized carbon of (C–H), (C–OH) and (C–O-C) groups. It is known that graphitic structures exposed to high temperature are more inclined to adsorb moistures upon interaction with the atmosphere via the highly active graphene sites (e.g., defects and edges) [43]. However, the portion of sp^2–hybridized carbon is larger than sp^3-counterpart carbon indicating the quality of the fabricated graphene. Moreover, the shake–up energy loss was identified as a very low intensity peak at ~289.4 eV [44]. Using Casa XPS software, the atomic concentrations were calculated revealing that carbon represents 98.37% of the entire sample, while oxygen represents only 0.97%. Overall, the spectra of VG 300, VG 400 and VG 500 samples appeared identical. No major chemical shifts or asymmetry in the carbon and oxygen peaks could be distinguished for all samples. The growth conditions in our experiments did not promote the formation of Si-C alloy (carbides) at the SiO_2/nano-graphite junction.

3.2. Raman

In general, the presence of G bands proves the graphitic nature of the fabricated material, while the presence of symmetrical 2D bands confirms the formation of graphene structure. On the other hand, the first-order D-peak does not appear in pristine graphene samples due to crystal symmetries [45].

In order to evaluate the carbon bonding structure of the resultant GNWs, Raman spectra were attained and displayed in Fig. 3. All samples showed D, G and 2D bands confirming the creation of multilayer graphene structures.

D-peak is generated when a charge carrier is excited and inelastically scattered by an adjacent phonon, then a second elastic scattering must be achieved by an existing defect (or zone boundary) to cause a recombination. This turns out to be Raman active peak after neighboring sp^2 carbons are transformed into sp^3-hybridization [29,46]. D-band is indexed to zone-boundary phonons owing to disorders (e.g., edges, fullerene-like structure, defects, and folds) in graphene material [8]. In Fig. 3 b & c, a sharp D-peak appeared at 1339 cm^{-1} and 1338 cm^{-1} for VG 400 and VG 500 samples, respectively. VG 300 samples showed a very weak/broad D-peak at 1341 cm^{-1}. This suggested that more defective graphene structures were formed at lower power of synthesis, with a higher quantity of defects and open edges. It is worth to mention that D-band may show higher intensity when samples are measured near to the edge of the sample, where the incidence of higher defects probability is expected owing to abundance of exposed-graphene-ends (allowing elastic backscattering of electrons) [47].

G-peak is associated with an E_{2g} in-plane vibrational mode of sp^2-bonded carbon. G-peak of the VG 300 samples revealed low intensity and emerged at around 1588 cm^{-1}, indicating that the sample might involve nano-crystalline graphitic structures. The intensity of G-peak significantly enhanced and slightly shifted down with increasing the RF power to 400 W, emerging at 1567 cm^{-1} and suggests the improvement in crystallinity degree. The position of G-peak further shifted down for VG 500 appearing at 1574 cm^{-1}. The absence of the D'-peak for all samples was also evident. D'-peak is related to the finite sp^2 crystallite size, and appears on the G-peak as a small peak [8]. In some cases, the D'-band does not appear in the Raman spectra due to the exposure of growing graphene to energetic plasma species, which previously reported on PECVD graphene syntheses [38].

2D-peak is generated from the second order of the zone-boundary phonons, typically linked to the number of the fabricated layers (stacking order) in the graphene matrix. The broadening of 2D-peak and its position shifts up with the increase of graphene layers. The VG 300 samples exhibited very low magnitude of 2D-peak in the Raman spectra at 2686 cm^{-1}, which implies a high degree of amorphous carbon structure [48]. With increasing processing power for VG 400 and VG 500 samples, significant 2D-peaks appeared at 2669 cm^{-1} and 2673 cm^{-1}, respectively. The drastic increases in the intensity of the 2D-band confirms the growth of VG walls on the given substrate.

The I_D/I_G ratio reflects the structural quality of graphene, as the crystallinity of the sample enhances when the I_D/I_G decreases. The I_D/I_G ratio of VG 300 was calculated to be 1.24, indicating the presence of defects in the formed graphene [38]. At higher power of deposition, VG 400 and VG 500 samples, the I_D/I_G ratio was 0.87 and 0.89, respectively. Hence, the graphene nanowalls produced at 400 W showed a relatively less disordered structure compare to VG 300 sample. Furthermore, I_D/I_G ratio can be employed to estimate graphene grain size based on the following relation: $L_a = C(\lambda) \times (I_D/I_G)^{-1}$, where La is grain size, λ is the wavelength of employed laser, and $C(\lambda)$ is a constant estimated through the equation $C(\lambda) = (2.4 \times 10^{-10}) \times \lambda^4$ [49,50]. The grain size was determined as 16.7 and 19.6 nm for VG 300 and VG 400 samples, respectively. The grain size in this study is comparable to typical GNWs reported in the literature. For example Khalid et al. observed that when the plasma power increases, the graphene grain size also increases, showing 21 and 23 nm for different growth temperatures [51]. Using PECVD at extremely low growing temperature (<560 °C), Zhang et al. measured the crystallite size to be between 9.6 and 18.0 nm for different growth periods [52]. Manojkumar et al. found that the PECVD-graphene grain size is 17 nm [53], and Mohd. Saman et al. reported a relatively small crystallite size in the range of ~7.5 nm for PECVD-graphene [54]. It is reasonable to say that the results of the grain size reported in this study are in good agreement with previous findings.

The I_{2D}/I_G ratio was calculated to be 0.32, 0.73 and 0.77 for VG 300, VG 400, and VG 500, respectively, indicating an increase in the number of graphene layers with increasing RF power. The associated full width at half maximum (FWHM) of the 2D peak was around 116, 80 and 74 cm^1 for VG 300, VG 400, and VG

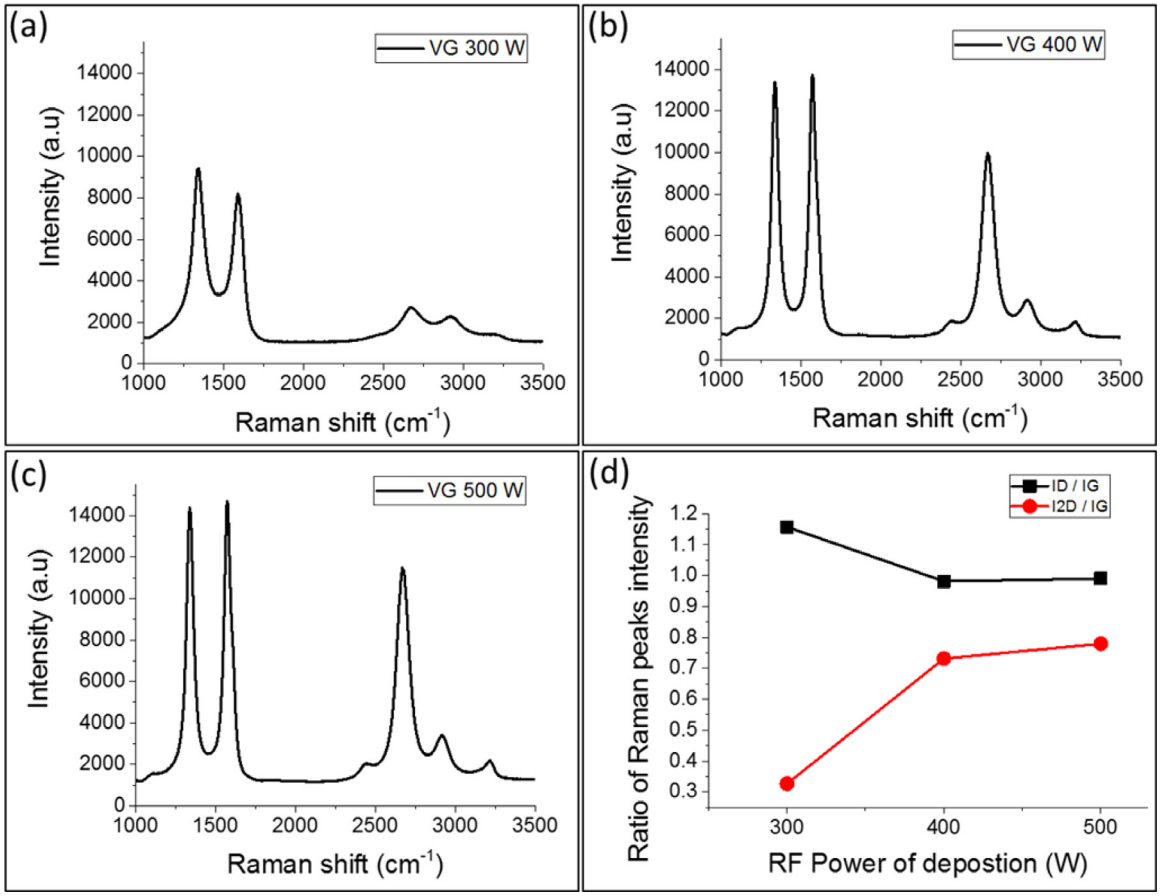

Fig. 3. Raman spectra of the VG films fabricated at different growth RF powers, with respective ID/IG and I2D/IG values.

500, respectively. From the values of the I_{2D}/I_G intensity ratios and FWHM, it is possible to confirm the formation of few layered graphene samples.

It is evident from the Raman spectra that the structures produced are highly dependent on the applied RF power. While VG 300 samples were more amorphous and revealed high defects, Raman spectra of VG 400 and VG 500 are very similar (both samples have very-close values of I_D/I_G and I_{2D}/I_G). This indicates that the graphene synthesized at 400 and 500 W had almost similar structural properties. However, SEM observations in Fig. 2c showed that the substrate was only fully covered by graphene in the case of samples produced at 500 W. It can be understood that increasing the RF power from 400 to 500 W had trivial influence on the structural properties and at the same time major influence on the growth rate of the formed graphene. Due to the strain energy at the edges and/or defects of early formed graphene at 400 W, the intermediate layer might be incapable to continue to grow bulk crystal, which triggers a transition from horizontal 2D complete films to discontinued 3D nano-islands observed by SEM. The increase in plasma power (300 to 500 W) increased the decomposition rates, temperature, momentum and density of generated ions, electrons and other energetic species [30]. Accordingly, much higher growth rate of graphene occurred and completely covered the surface.

3.3. AFM and contact angle

Typical 3D AFM images with associated height profiles for VG 300, VG 400, and VG 500 samples are presented in Fig. 4. The related quantitative analyses of topographical parameters for these samples are summarized in Table 1. For VG 300 samples, topographic parameters measured as: average roughness (S_a = 4.1 ± 0.6 nm), root mean square (S_q = 5.6 ± 0.3 nm) and maximum peak height (S_m = 28.6 ± 1.7 nm). With increasing RF power to 400 W, those parameters slightly increased to S_a = 5.2 ± 0.8 nm, S_q = 6.6 ± 0.5 nm, and S_m = 61.0 ± 3.1 nm. At RF power of 500 W, roughness parameters increased significantly to S_a = 43.9 ± 7.2 nm, S_q = 57.3 ± 5.4 nm and S_m = 410.8 ± 17.8 nm. Moreover, the corresponding line spectrum of VG 500 samples in Fig. 4c clearly shows nano-protrusion-like structures presented on the graphene sample. These protrusions could appeared from curved edges, flakes and folding that typically take place during the formation of graphene layers by PECVD. AFM indicated that the protrusions have, on average, a width of few tens nanometers and heights of few hundreds nanometers, signifying the presence of ultra-thin and sharp edges on the surface of the sample, as demonstrated by the SEM observations in Fig. 2d. These topographical structures are commonly detected in vertical oriented graphene; for instance Wei et al. recently reported a similar surface profile of vertical graphene involving sharp protrusions with heights around 250 nm grown on SiO_2 substrates [15]. The

Table 1
Surface roughness profiles for VG samples acquired using AFM at scanning area of 5 μm × 5 μm.

Roughness parameter	VG 300	VG 400	VG 500
Average Roughness, S_a (nm)	4.1 ± 0.6	5.2 ± 0.8	43.9 ± 7.2
Root Mean Square, S_q (nm)	5.6 ± 0.3	6.6 ± 0.5	57.3 ± 5.4
Max Surface, S_m (nm)	28.6 ± 1.7	61.0 ± 3.1	410.8 ± 17.8
Surface skewness, S_{sk}	4.4 ± 0.3	2.8 ± 0.4	1.5 ± 0.2
Coefficient of kurtosis, S_{ka}	3.6 ± 0.6	3.8 ± 0.1	2.1 ± 0.3

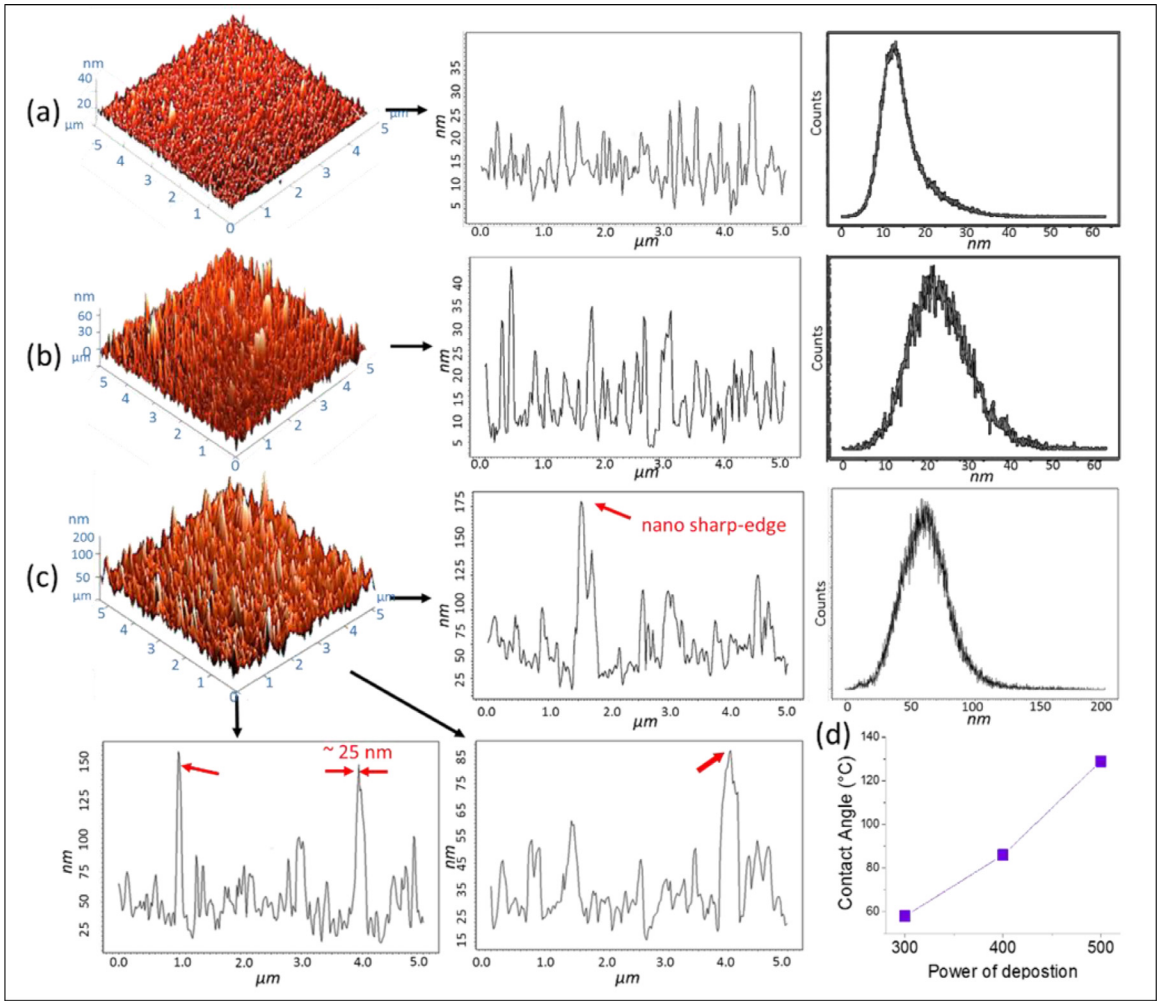

Fig. 4. a, b & c AFM 3D images, corresponding surface profiles and heights distributions of VOGNs samples fabricated at different RF powers. (d) static water contact angle on VOGNs surfaces.

quantitative roughness values for VG 500 samples are also in a good agreement with previously published reports. Akbari et al. reported roughness parameters of S_a = 47.84 nm, S_q = 62.16 nm and S_m = 226.6 nm for graphene produced at 400 W using electron cyclotron resonance–chemical vapor deposition system (ECR-CVD) [55]. Gao et al. reported different values of the root mean square roughness (S_q = 95, 100 and 112 nm) for PECVD-graphene fabricated at 400 W at different base pressures [56]. A roughness (S_a) of 68.56 nm was also reported by Abidinet et al. for vertical graphene fabricated at 40 W and 1000 °C [57]. Further studies found the roughness parameter (S_m) of vertically oriented graphene nanohills to be 31 nm, with an average height of 15 nm [58]. However, compared to stacked 2D graphene, the vertically oriented graphene has specific features such as high surface area, great roughness degree and very long edges giving exclusive functionalities. Such a property would facilitate its integration in low-cost, eco-friendly, self-cleaning surfaces.

Surface skewness parameter (S_{sk}) can be used to further define the distribution of the presented protrusions on the graphene surfaces with respect to the mean line. Surface skewness measures the irregularity of deep valleys or high peaks determining the symmetry of the deviations of a surface configuration. All samples in this study were found to be positively skewed, and the maximum value of skewness was found to be 4.4 nm for VG 300 sample. In addition, surface kurtosis (S_{ka}) was used to describe the distribution of the protrusions, where distributions with positive kurtosis are considered by high peaks, while distributions with negative kurtosis are characterized by flat-topped curves. We observed samples produced at 400 W possessed relatively higher kurtosis value (S_{ka} > 3), indicating a more spread-out height distribution for these surfaces compared to other samples. Samples fabricated at 500 W revealed considerably different values of S_{sk} and S_{ka}, which is likely that the distribution of peaks on the substrate, rather than their entire magnitude, may play an important role in the shaping of the morphology of the graphene. We assume that the surface of VG 500 is largely dominated by high peaks with irregular great deviations from the main line. It can also be observed that skewness and kurtosis factors of all VOGNs samples in this study did not follow a specific pattern with the respective to the applied RF power.

Static water contact angle data were recorded for VOGNs samples on a minimum of three points for all samples. SiO_2 used as substrates possessed water contact angles around 35 °. In each test, the drop profile was acquired for 60 s by video camera and numerically solved. As presented in Fig. 4d, the mean water contact angle for VOGNs surfaces were measured to be 65, 90 and 123 ° for VG 300, VG 400 and VG 500, respectively. The fabricated graphene significantly changed the hydrophilic nature of the SiO_2 substrates to a hydrophobic surface, where the applied RF power played an important role on the resultant wettability of graphene. The high value of contact angle for VG 500 indicates that a high ratio of sp^2-hybridized bonding (as demonstrated by Raman) and electrons

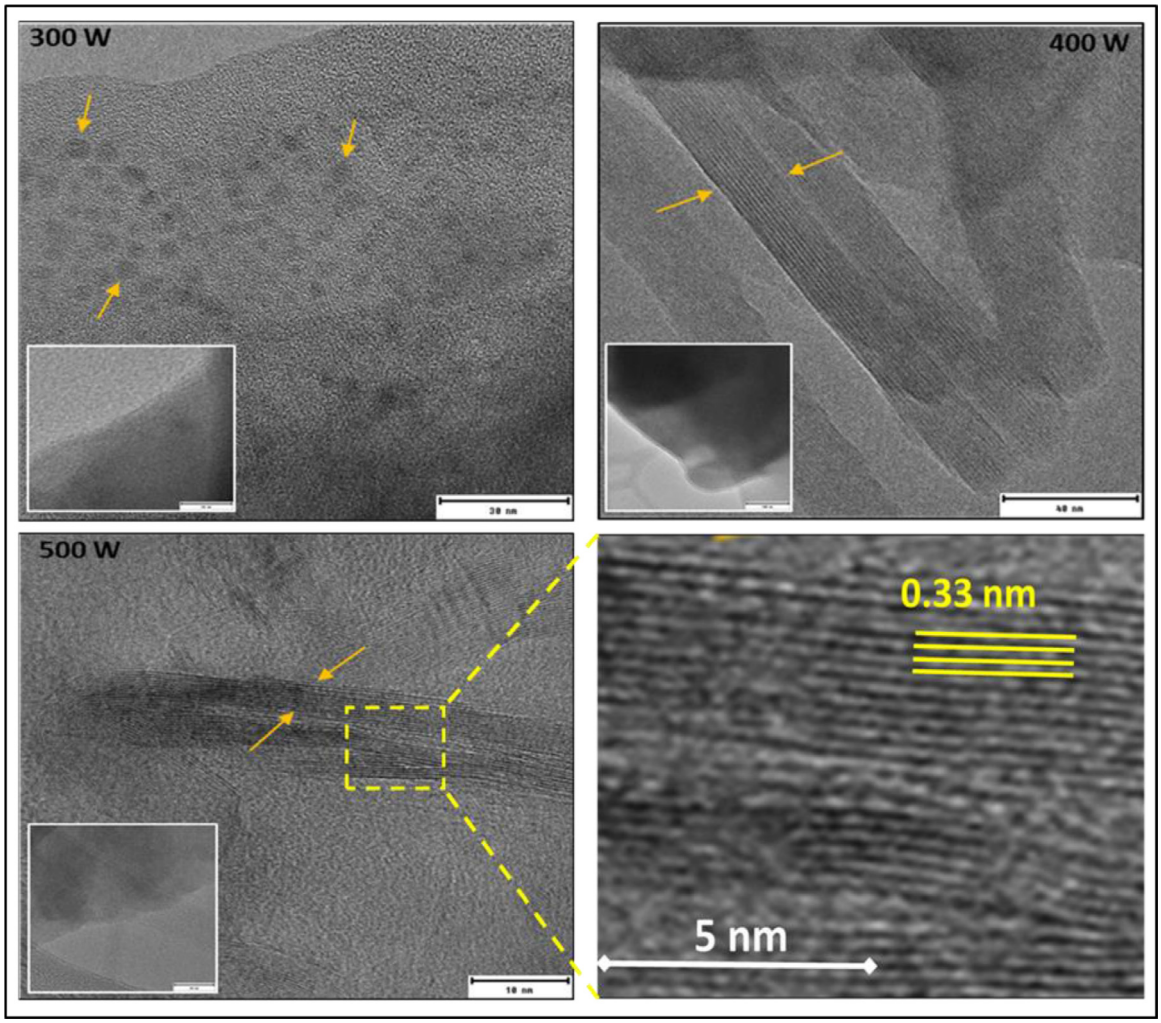

Fig. 5. TEM images of VOGNs samples fabricated at 300, 400 and 500 W, insets show high resolution images with the lattice spacing value for the resultant graphene films.

coupling effects enhanced the repellent of polar liquids like water. Furthermore, the cavities formed by interweaved graphene walls could effectively participate into the hydrophobic surface performance [59]. A similar dependency of graphene wettability on applied power was observed by Bayram et al., since they reported contact angles to be 86, 99 and 102° for increased RF power in a PECVD system [60]. The wettability can be adjusted depending on the RF power of graphene fabrication, which can be used in many useful applications such as self-cleaning windows and water collection devices.

The stable electronic structure of graphene results in a relatively low surface energy. The attraction from the non-polar lattice to water molecules is weaker than the binding energy among water molecules [50]. Consequently, the roughness and the surface chemistry of the graphene walls produce a highly hydrophobic surface. It is worth to mention that the roughness can result in the increase in the wettability of the graphene surfaces. According to Wenzel equation, rougher surfaces will produce a larger contact angle [56]; accordingly the increase in the wettability with a higher RF power in this study could be also attributed to the higher surface roughness with the increasing power of deposition. However, the wetting behavior of graphene broadly depends on interconnected effects of several extrinsic and intrinsic elements including chemical structure, topography, layers number, oxygen functionality, crystallinity and defects [61, 62].

Though hydrophobic or hydrophilic characteristics of graphene may not be primarily responsible for the enhanced mechano-bactericidal activity of vertically oriented graphene, they may play an important role in determining the adhesion forces between bacterial cells and graphene nanosheets. Studies have demonstrated that hydrophobic graphene prevents bacterial adhesion on the surface of the materials [63]. In another study, it was shown that *P. fluorescent* cells have stronger adhesion on horizontal graphene oxide as compared to randomly oriented graphene having vertical and exposed edges [64].

3.4. Transmission electron microscopy (TEM)

SEM images represented the 3D organization of graphene nanowalls on the surface of the substrate. In order to unveil the features in graphene lattice, transmission electron microscopy (TEM) was performed. TEM images in Fig. 5 (high resolution images in insets) show the quality of the lattice, the interlayer spacing, and also the formation of what appears to be nano-onions incorporated into graphene sheets. The interesting phenomenon of nano-onion formation (observed in Fig. 5a) has been already reported by Alancherry et al. [35], where they also used PECVD to grow graphene film. The unique features of PECVD i.e., high-energy ionic collisions and high temperature are responsible for this simultaneous occurrence of deposition of graphene lattice and its defects, which is otherwise achieved through multiple stages including post-synthesis treatment. The nano-onions in our experiments are approximately 10 nm or less in sizes. The TEM images of 400 W and 500 W (Fig. 5a and b) clearly showed that the graphene is a

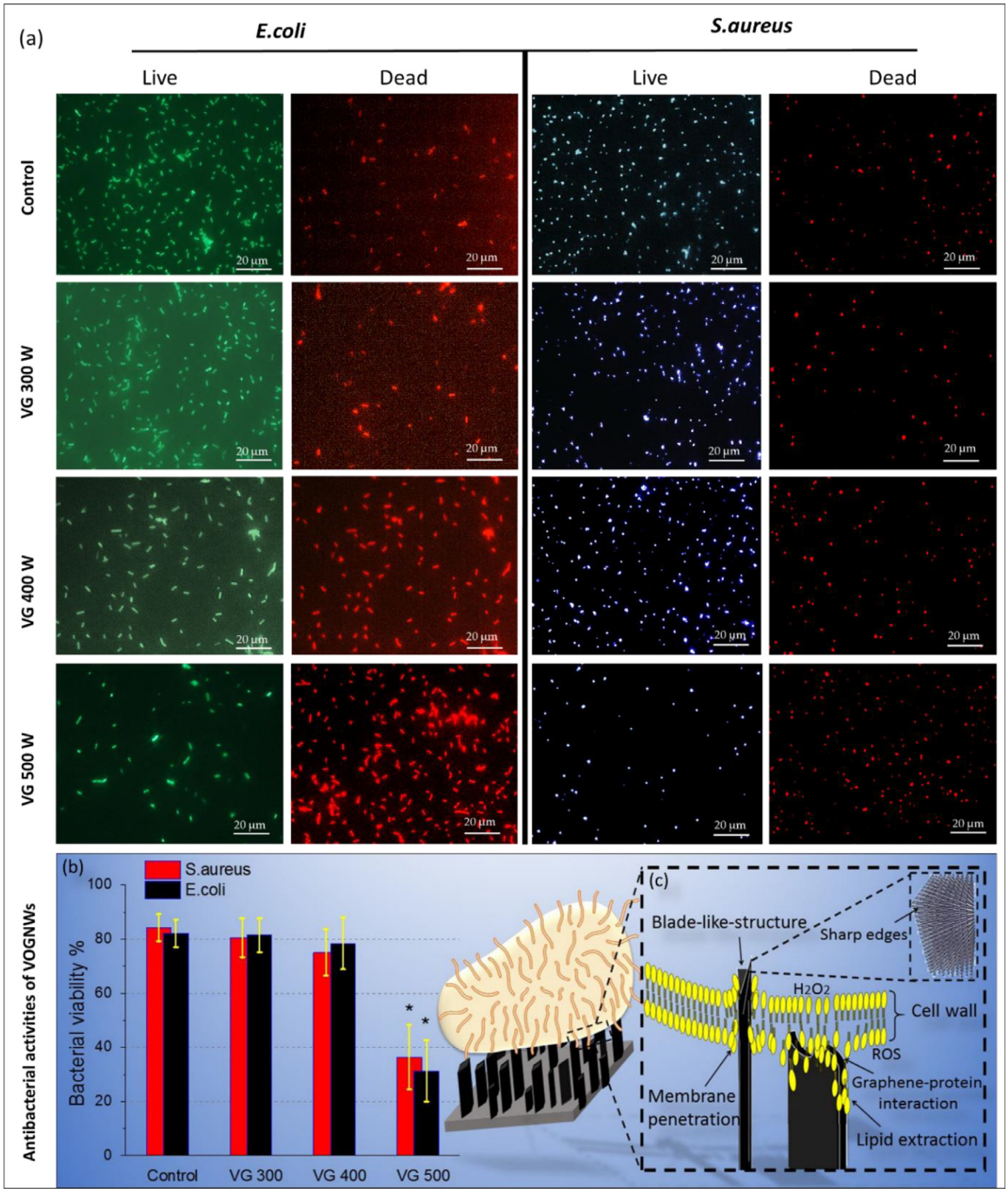

Fig. 6. Antimicrobial activities of vertically grown graphene nanowalls produced by PECVD against *E. coli* and *S. aureus* bacteria; (a) confocal scanning laser microscopy visualizations (magnification of 63 X), where viable cells appeared green and dead cells appeared red stained by Invitrogen Dead/Live Kit; (b) statistical analysis displays the antibacterial outcomes of different graphene samples and quartz controls. The given data represent means ± SD ($n = 3$); (c) proposed antimicrobial mechanism of VG samples through the physical damages to the microbial cell wall membrane by ultra-thin graphene sharp structures presented on the surface (For interpretation of the references to color in this figure legend, the reader is referred to the web version of this article.).

multi-layered structure with lattice spacing (0.33 nm) that is comparable to previous reports on graphene structures fabricated by PECVD [35,65,66].

3.5. Bacterial toxicity

The antibacterial effectiveness of VOGNs samples was evaluated against rod-shaped *E. coli* (gram-negative cell) and round-shaped *S. aureus* (gram-positive cell) in terms of bacteria viability using Live/Dead cell confocal imaging. The ratio of live bacterial cell against the total number of bacteria (both live and dead cells) was determined to calculate the antibacterial performance of the graphene. Bactericidal effectiveness of VG samples against *E. coli* bacteria is presented in Fig. 6a. After a 24 h incubation period, bacterial cells were able to attach and normally grow on the surface of control (quartz), VG 300 and VG 400, whereas VG 500 samples revealed considerable bacterial toxicity.

CLSM images clearly showed a much higher average number of dead bacterial cells on the surfaces of VG 500 samples compared to all other sample groups. As displayed in Fig. 6b, *E. coli* cell viability

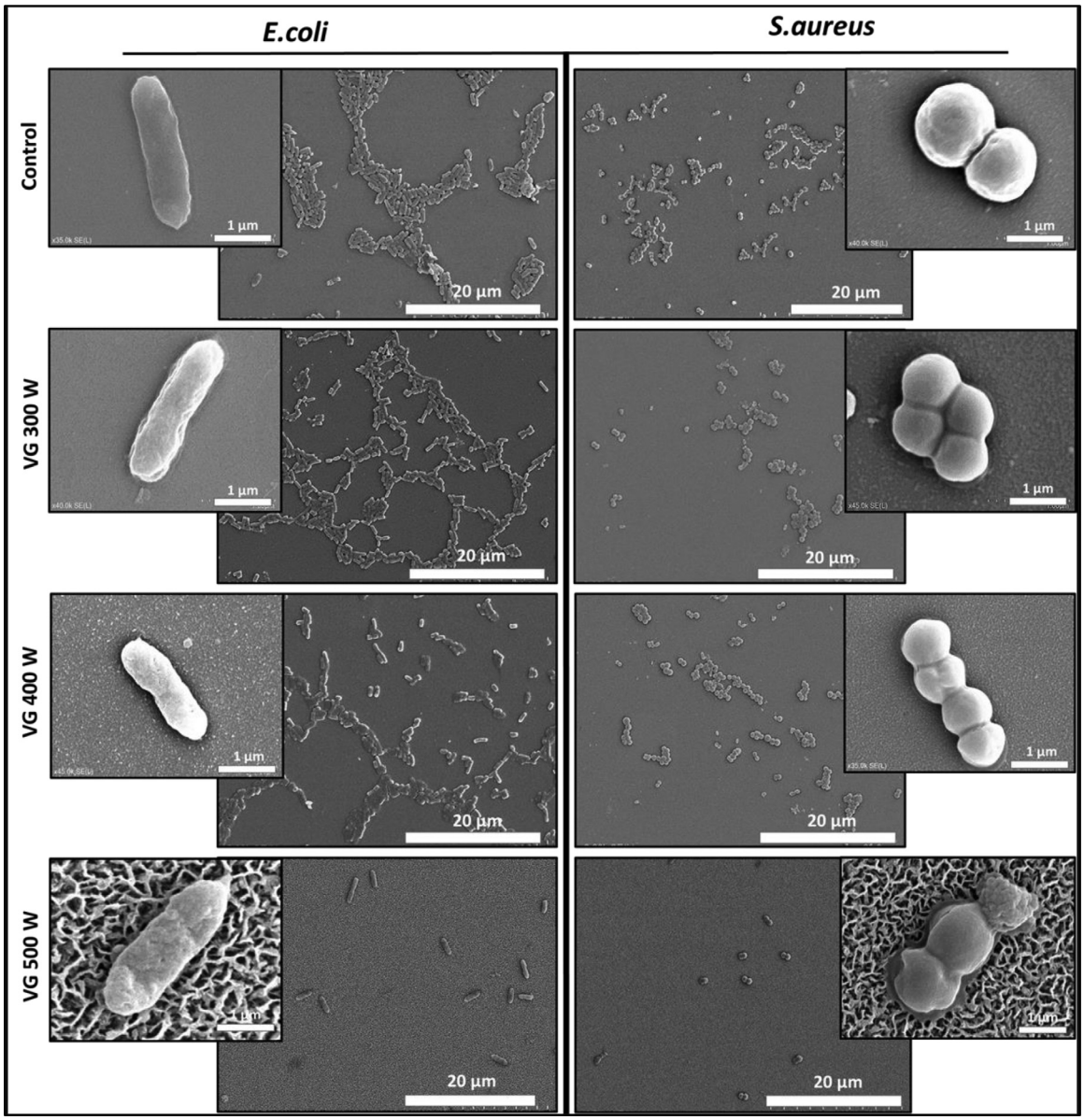

Fig. 7. SEM of *E. coli* and *S. aureus* grown on quartz control and vertically oriented graphene samples produced at different RF power. The incubation time is 24 h, at temperate of 37 °C.

was estimated to be approximately 82%, 81%, 78%, and 33% when cultured on the surfaces of control, VG 300, VG 400 and VG 500 samples, respectively. This illustrates a significant reduction in the number of live bacterial cells when exposed to vertical graphene nanowalls. Similarly, the viability of *S. aureus* pathogen cells was approximately 84%, 80%, 74%, and 37% when cells were cultured on the surfaces of control, VG 300, VG 400 and VG 500 samples, respectively.

To further investigate the antimicrobial activities of VOGNs materials, microbial morphologies of incubated *E. coli* and *S. aureus* microorganisms (24 h incubation time) were observed by SEM. Fig. 7 shows that pathogens incubated on surfaces of control, 300 and 400 W were intact, since they revealed structure integrity with no noticeable damage to the bacterial body. In contrast, a large fraction of cells attached to the VG 500 surfaces had significant morphological changes, where microbial cell walls appeared abnormal, deformed and pimply. The cell wall damage indicates that the sharp edges and blade-like structures of VOGNs might severely injure and/or penetrate microbial membranes. This observation points toward biological death followed to the affected microorganism upon direct exposure to VG 500. Yet, several dead bacteria (that remain on the surface of the sample) may cover the graphene walls immediately under their surface, serving as a potential safe platform for other planktonic cells to attach from the above liquid phase [16]. Although some cells on VG 500 appeared unharmed/intact, a quantitative evaluation of SEM data suggest that physical damage to a large number of bacterial cells occurred in both gram negative and gram positive cells, as shown in Fig. 7 for VG 500. Our findings are in a good agreement with recently accomplished studies. For example, a recent report showed that bacteria suffered various stress activities (e.g., DNA damage or inhibition of replication) during attachment to vertical graphene films grown by PECVD [15]. Similarly, Lu et al. observed that vertically oriented graphene oxide nano-sheets revealed a substantially higher degree of antibacterial performance against bacterial cell, compared to randomly oriented and horizontal graphene [11]. They noticed that antibacterial performance of VG structures comes from an increased density of edges with a preferential align-

ment for bacterial membrane distraction [11]. Pandit et al. also found that the edges of vertically aligned graphene flakes (heights of 60 and 100 nm) were able to roughly penetrate microbial membranes and drain the cytosolic content, with cells incapable to develop resistance upon multiple exposures [16]. Further studies emphasized the importance of sharply-edged structures of graphene to significantly inhibit different microorganisms (e.g., viruses) upon direct interaction [67]. The roughness of graphene also affects its antibacterial performance since the antibacterial performance of graphene oxide films is governed by the relative surface roughness with respect to the microbial size [21].

As shown in Fig. 6b, VG 500 samples revealed a slightly higher antibacterial efficacy against *E. coli* than *S. aureus*. This can be attributed to inherent differences in the cell wall composition in gram-negative and gram-positive microorganisms. A gram-positive cell has a thick peptidoglycan layer that consists of teichoic and lipoteichoic acids, while a gram-negative cell has a thin peptidoglycan layer and a superficial membrane that consists of lipopolysaccharides, phospholipids, and proteins [14,68]. Even though gram-negative cells have a much thinner layer of peptidoglycan, they have an additional layer of the outer membrane [69]. Hence, a gram-negative cell (*E. coli*) retains a stiffer envelop that affords more resistance to the sharp edges of vertical graphene, compared to a gram-positive cell (*S. aureus*). Some researchers had reported a similar tendency of difference between bacterial species in responding to graphene nanomaterials [15]. Nonetheless, other studies revealed that graphene nanostructures are more toxic to gram-negative bacteria than gram-positive bacteria [70].

Apart from the physical effects of VG structures, the interaction between VG surfaces and microorganisms can cause chemical oxidation to bacterial biomolecules, involving the formation of toxic reactive oxygen species (ROS). High concentrations of ROS (e.g., singlet molecular oxygen and superoxide anions) induced by graphene can lead cells to enter a state of oxidative stress, causing extra destruction to microbial cellular components such as DNA, lipids, proteins and gradual degeneration of cell membrane [70,71]. However, it has been proposed that the graphene may extract phospholipid molecules from the lipid layers of the membranes triggering distortion and irreversible damage of the cell membrane [19], as illustrated in Fig. 6.c. It is clear that the deactivation mechanism of graphene materials is still controversial. This is probably because graphene could be prepared with very dissimilar properties (e.g., size, layers number, morphology, presence of oxygen, electronic configuration, hydrophilicity, quality, defect density, etc.) that make it challenging to predict a precise antimicrobial model/mechanism [14,21]. However, our findings emphasize the effectiveness of sharp edges of vertically oriented graphene to yield irreversible physical damages in microorganisms. Perhaps, synergistic effects introduced by the surface roughness and distinctive sharp topographical features along with the hydrophilic nature of the VG 500 surface contributed to the observed antimicrobial characteristics. Indeed, further in-depth experiments are required to shed more light on the influence of different topographical features of VG surfaces on the antibacterial outcome.

4. Conclusion

Vertically oriented graphenes present a particularly attractive material platform for the control of cell-surface interactions as they maximize the exposure of the cells to the graphene reactive edges. Uniform vertical graphene walls from *Pelargonium graveolens* extract is synthesized using single-step, well-controlled and catalyst-free PECVD. Raman spectra confirmed the graphene presence and indicated that more defective graphene structures were created at lower fabrication power. SEM imaging showed the gradual evolution of interconnected graphene wall networks on the surface of the substrate, with well-resolved architectures formed at 500 W, where the average length of each wall is ~150 to 300 nm, and the width is ~10 to 40 nm. XPS confirmed that the level of sp^2–hybridization was characteristic of high-quality graphene, with the atomic fractions of carbon and oxygen at 98.37% and 0.97%, respectively. The fundamental characteristics showed that the graphene is of good quality and is vertically aligned. The VG graphene exhibited hydrophobic characteristics and high surface roughness values. The antibacterial performance of the material was demonstrated toward important human pathogens. Our data emphasizes the physical nature of the observed bactericidal effects of vertically oriented graphene performing as a knife-edge to damage the bacterial cell membrane. The developed graphene has shown an impressive potential in tackling various aspects of microbial infections in antibacterial surface applications.

Declaration of Competing Interest

There is no conflict of interest

References

[1] W. Choi, et al., Synthesis of graphene and its applications: a review, Crit. Rev. Solid State Mater. Sci. 35 (1) (2010) 52–71.
[2] F. Bonaccorso, et al., Graphene, related two-dimensional crystals, and hybrid systems for energy conversion and storage, Science 347 (6217) (2015) 1246501.
[3] A.V. Prydatko, et al., Contact angle measurement of free-standing square-millimeter single-layer graphene, Nat. Commun. 9 (1) (2018) 4185.
[4] E. Kusiak-Nejman, A.W. Morawski, TiO_2/graphene-based nanocomposites for water treatment: a brief overview of charge carrier transfer, antimicrobial and photocatalytic performance, Appl. Catal. B 253 (2019) 179–186.
[5] B. Ouyang, et al., Green synthesis of vertical graphene nanosheets and their application in high-performance supercapacitors, RSC Adv. 6 (28) (2016) 23968–23973.
[6] J. Chen, Z. Bo, G. Lu, in: Vertically-Oriented Graphene, Springer International Publishing Switzerland, 2015, pp. 978–983. DOI10.
[7] S. Mao, et al., Direct growth of vertically-oriented graphene for field-effect transistor biosensor, Sci. Rep. 3 (1) (2013) 1–6.
[8] Z. Bo, et al., Plasma-enhanced chemical vapor deposition synthesis of vertically oriented graphene nanosheets, Nanoscale 5 (12) (2013) 5180–5204.
[9] N.G. Shang, et al., Catalyst-free efficient growth, orientation and biosensing properties of multilayer graphene nanoflake films with sharp edge planes, Adv. Funct. Mater. 18 (21) (2008) 3506–3514.
[10] O. Akhavan, E. Ghaderi, Toxicity of graphene and graphene oxide nanowalls against bacteria, ACS Nano 4 (10) (2010) 5731–5736.
[11] X. Lu, et al., Enhanced antibacterial activity through the controlled alignment of graphene oxide nanosheets, Proc. Natl. Acad. Sci. (2017) 201710996.
[12] M.D. Rojas-Andrade, et al., Antibacterial mechanisms of graphene-based composite nanomaterials, Nanoscale (2017).
[13] M.A. Gacem, H. Gacem, A. Ould-El-Hadj-Khelil, *Nanocarbons: antibacterial, antifungal, and antiviral activity and the underlying mechanism*„ in: Carbon Nanomaterials for Agri-Food and Environmental Applications, Elsevier, 2020, pp. 505–533.
[14] A. Al-Jumaili, et al., Review on the antimicrobial properties of carbon nanostructures, Materials 10 (9) (2017) 1066 (Basel).
[15] W. Wei, et al., Distinct antibacterial activity of vertically aligned graphene coating against gram-positive and gram-negative bacteria, J. Mater. Chem. B 8 (2020) 6069–6079.
[16] S. Pandit, et al., Vertically aligned graphene coating is bactericidal and prevents the formation of bacterial biofilms, Adv. Mater. Interfaces 5 (7) (2018) 1701331.
[17] K. Prasad, et al., Effect of precursor on antifouling efficacy of vertically-oriented graphene nanosheets, Nanomaterials 7 (7) (2017) 170.
[18] H.E. Karahan, et al., Graphene materials in antimicrobial nanomedicine: current status and future perspectives, Adv. Healthc. Mater. 7 (13) (2018) 1701406.
[19] Y. Tu, et al., Destructive extraction of phospholipids from Escherichia coli membranes by graphene nanosheets, Nat. Nanotechnol. 8 (8) (2013) 594–601.
[20] V.T. Pham, et al., Graphene induces formation of pores that kill spherical and rod-shaped bacteria, ACS Nano 9 (8) (2015) 8458–8467.
[21] F. Zou, et al., Wrinkled surface-mediated antibacterial activity of graphene oxide nanosheets, ACS Appl. Mater. Interfaces 9 (2) (2017) 1343–1351.
[22] W. Wei, et al., Distinct antibacterial activity of a vertically aligned graphene coating against Gram-positive and Gram-negative bacteria, Journal of Materials Chemistry B 8 (28) (2020) 6069–6079.
[23] G. Yuan, et al., Graphene sheets via microwave chemical vapor deposition, Chem. Phys. Lett. 467 (4–6) (2009) 361–364.
[24] O. Bayram, A study on 3D graphene synthesized directly on Glass/FTO substrates: its Raman mapping and optical properties, Ceram. Int. 45 (14) (2019) 16829–16835.
[25] J. Zhao, et al., A growth mechanism for free-standing vertical graphene, Nano Lett. 14 (6) (2014) 3064–3071.

[26] K. Bazaka, et al., Anti-bacterial surfaces: natural agents, mechanisms of action, and plasma surface modification, RSC Adv. 5 (60) (2015) 48739–48759.
[27] A. Al-Jumaili, et al., Eco-friendly nanocomposites derived from geranium oil and zinc oxide in one step approach, Sci. Rep. (2019) 9.
[28] A. Al-Jumaili, et al., Electrically insulating plasma polymer/ZnO composite films, Materials 12 (19) (2019) 3099 (Basel).
[29] D.H. Seo, et al., Plasma break-down and re-build: same functional vertical graphenes from diverse natural precursors, Adv. Mater. 25 (39) (2013) 5638–5642.
[30] S. Alancherry, et al., Tuning and fine morphology control of natural resource-derived vertical graphene, Carbon 159 (2020) 668–685 N Y.
[31] K. Bazaka, M.V. Jacob, K. Ostrikov, Sustainable life cycles of natural-precursor-derived nanocarbons, Chem. Rev. 116 (1) (2015) 163–214.
[32] D. Seo, et al., Vertical graphene gas-and bio-sensors via catalyst-free, reactive plasma reforming of natural honey, Carbon 60 (2013) 221–228 N Y.
[33] Y. Wang, et al., MoS 2-coated vertical graphene nanosheet for high-performance rechargeable lithium-ion batteries and hydrogen production, NPG Asia Mater. 8 (5) (2016) e268–e269.
[34] S. Kumar, et al., Oriented graphenes from plasma-reformed coconut oil for supercapacitor electrodes, Nanomaterials 9 (12) (2019) 1679.
[35] S. Alancherry, et al., Fabrication of nano-onion structured graphene films from citrus sinensis extract and their wetting and sensing characteristics, ACS Appl. Mater. Interfaces (2020).
[36] A. Wu, et al., Upcycling waste lard oil into vertical graphene sheets by inductively coupled plasma assisted chemical vapor deposition, Nanomaterials 7 (10) (2017) 318.
[37] A. Al-Jumaili, et al., *Plasma treatment of polymeric membranes*„ in: Non-Thermal Plasma Technology for Polymeric Materials, Elsevier, 2019, pp. 211–240.
[38] M.V. Jacob, et al., Catalyst-free plasma enhanced growth of graphene from sustainable sources, Nano Lett. 15 (9) (2015) 5702–5708.
[39] A. Al-Jumaili, K. Bazaka, M. Jacob, Retention of antibacterial activity in geranium plasma polymer thin films, Nanomaterials 7 (9) (2017) 270.
[40] M. Jalali-Heravi, B. Zekavat, H. Sereshti, Characterization of essential oil components of Iranian geranium oil using gas chromatography-mass-spectrometry combined with chemometric resolution techniques, J. Chromatogr. A 1114 (1) (2006) 154–163.
[41] Scientific, T.F.*LIVE/DEAD® baclight bacterial viability kits*. 2004; Available from: https://assets.thermofisher.com/TFS-Assets/LSG/manuals/mp07007.pdf.
[42] O. Baranov, et al., Formation of vertically oriented graphenes: what are the key drivers of growth? 2D Materials 5 (4) (2018) 044002.
[43] K. Ganesan, et al., A comparative study on defect estimation using XPS and Raman spectroscopy in few layer nanographitic structures, Phys. Chem. Chem. Phys. 18 (32) (2016) 22160–22167.
[44] D.H. Seo, et al., Structure-controlled, vertical graphene-based, binder-free electrodes from plasma-reformed butter enhance supercapacitor performance, Adv. Energy Mater. 3 (10) (2013) 1316–1323.
[45] I. Childres, et al., Raman spectroscopy of graphene and related materials, New Dev. Photon Mater. Res. 1 (2013) 1–20.
[46] A. Eckmann, et al., Probing the nature of defects in graphene by Raman spectroscopy, Nano Lett. 12 (8) (2012) 3925–3930.
[47] C. Casiraghi, et al., Raman spectroscopy of graphene edges, Nano Lett. 9 (4) (2009) 1433–1441.
[48] R. Rozada, et al., Controlled generation of atomic vacancies in chemical vapor deposited graphene by microwave oxygen plasma, Carbon 79 (2014) 664–669 N Y.
[49] L. Cançado, et al., General equation for the determination of the crystallite size L a of nanographite by Raman spectroscopy, Appl. Phys. Lett. 88 (16) (2006) 163106.
[50] C. Yang, et al., Direct PECVD growth of vertically erected graphene walls on dielectric substrates as excellent multifunctional electrodes, J. Mater. Chem. A 1 (3) (2013) 770–775.
[51] A. Khalid, M.A. Mohamed, A.A. Umar, Graphene growth at low temperatures using RF-plasma enhanced chemical vapour deposition, Sains Malays. 46 (7) (2017) 1111–1117.
[52] N. Zhang, et al., Direct synthesis of vertical graphene nanowalls on glass substrate for thermal management, Mater. Res. Express 5 (6) (2018) 065606.
[53] P. Manojkumar, et al., Role of process gas ratio on the structural and plasmonic properties of graphene nanowalls, Diam. Relat. Mater. 97 (2019) 107452.
[54] R. Mohd Saman, et al., High voltage graphene nanowall trench MOS barrier schottky diode characterization for high temperature applications, Appl. Sci. 9 (8) (2019) 1587.
[55] M. Akbari, et al., in: Characterization of vertically-oriented graphene nanosheets grown on copper substrate, 2020.
[56] J. Gao, et al., Superhydrophobic graphenic carbon nanowalls fabricated by one-step PECVD, Mater. Lett. 184 (2016) 273–277.
[57] H.E.Z. Abidin, et al., Growth time dependent of high quality graphene on interdigital electrodes for MEMS supercapacitor, in: Proceedings of the IEEE Regional Symposium on Micro and Nanoelectronics (RSM) 2017, IEEE, 2017.
[58] K. Akbar, et al., Superaerophobic graphene nano-hills for direct hydrazine fuel cells, NPG Asia Mater. 9 (5) (2017) e378–e379.
[59] H. Watanabe, et al., Control of super hydrophobic and super hydrophilic surfaces of carbon nanowalls using atmospheric pressure plasma treatments, Jpn. J. Appl. Phys. 51 (1S) (2012) 01AJ07.
[60] O. Bayram, O. Simsek, Vertically oriented graphene nano-sheets grown by plasma enhanced chemical vapor deposition technique at low temperature, Ceram. Int. 45 (11) (2019) 13664–13670.
[61] S.Y. Kim, et al., Substrate temperature effect on the growth of carbon nanowalls synthesized via microwave PECVD, Mater. Res. Bull. 58 (2014) 112–116.
[62] S. Ghosh, et al., Process-specific mechanisms of vertically oriented graphene growth in plasmas, Beilstein J. Nanotechnol. 8 (2017) 1658–1670.
[63] M. Muthu, et al., Hydrophobic bacteria-repellant graphene coatings from recycled pencil stubs, Arab. J. Sci. Eng. 43 (1) (2018) 241–249.
[64] J. Xue, et al., Bacterial adhesion to graphene oxide (GO)-functionalized interfaces is determined by hydrophobicity and GO sheet spatial orientation, Environ. Sci. Technol. Lett. 5 (1) (2018) 14–19.
[65] R. Kaindl, et al., Synthesis of graphene-layer nanosheet coatings by PECVD, Mater. Today Proc. 2 (8) (2015) 4247–4255.
[66] N. Wei, et al., Direct synthesis of flexible graphene glass with macroscopic uniformity enabled by copper-foam-assisted PECVD, J. Mater. Chem. A 7 (9) (2019) 4813–4822.
[67] B.J. Lee, S.C. Cho, G.H. Jeong, Atmospheric pressure plasma treatment on graphene grown by chemical vapor deposition, Curr. Appl. Phys. 15 (5) (2015) 563–568.
[68] T.J. Silhavy, D. Kahne, S. Walker, The bacterial cell envelope, Cold Spring Harb. Perspect. Biol. 2 (5) (2010) a000414.
[69] P. Eaton, et al., Atomic force microscopy study of the antibacterial effects of chitosans on Escherichia coli and Staphylococcus aureus, Ultramicroscopy 108 (10) (2008) 1128–1134.
[70] K. Krishnamoorthy, et al., Antibacterial efficiency of graphene nanosheets against pathogenic bacteria via lipid peroxidation, J. Phys. Chem. C 116 (32) (2012) 17280–17287.
[71] J. Li, G. Wang, H. Zhu, et al., Antibacterial activity of large-area monolayer graphene film manipulated by charge transfer, Sci Rep 4 (2014) 4359, doi:10.1038/srep04359.